

Low-Profile, Dual-Band, Unidirectional RFID Tag Antenna Using Metasurface

Thi Ngoc Hien Doan, Son Xuat Ta*, Van Khang Nguyen,
Khac Kiem Nguyen, and Chien Dao-Ngoc

Abstract—In this paper, a low-profile, dual-band, unidirectional, tag antenna is proposed for ultra-high frequency band (UHF) radio frequency identification (RFID) applications. The antenna consists of a compact printed dipole, a metasurface of 4×4 periodic metallic plates, and a metallic reflector. The dipole antenna is fed by a modified T-matching network for a conjugate impedance matching with the UCODE G2XM chip. The metasurface is designed to work as an artificial magnetic conductor surface, which allows low-profile configuration and unidirectional radiation. More interestingly, the finite-sized metasurface generates extra resonance for the antenna system, which is combined with dipole resonance for the dual-band operation. For an easy realization and low cost, the dipole and metasurface are built on the top and bottom sides of a thin FR-4 substrate, respectively. The final design with overall size of $190 \text{ mm} \times 190 \text{ mm} \times 15.8 \text{ mm}$ ($0.532\lambda \times 0.532\lambda \times 0.044\lambda$ at 840 MHz) yields a simulated $|S_{11}| < -10 \text{ dB}$ bandwidth of 840–855 MHz and 916–932 MHz and a unidirectional radiation with a directivity of 7.0 dB and 5.8 dB at 925 MHz and 845 MHz, respectively. The antenna has been fabricated and tested. The measured readable range agrees rather closely with the predicted values. The measurements result in the maximum readable range of 6-m and 4.4-m at standard frequency bands of FCC (902–928 MHz) for North America and IN (840–845 MHz) for India, respectively.

1. INTRODUCTION

Radio frequency identification (RFID) is a type of technology using electromagnetic fields to automatically identify and track tags attached to objects [1]. In general, an RFID system consists of a reader, many tags, and a host computer to connect to networks. Due to the simple configuration and easy match to different chips, dipole antennas are commonly used for designing RFID tags with a chip attached in the center. However, there are some drawbacks on the usage of the conventional RFID tags. One of the main limitations is caused by metals or human tissues. The performance of RFID tags decreases considerably when being placed on or close to metals, as well as human bodies. The degradation of performance is due to the material characteristics influencing fundamental antenna properties such as input impedance, gain, and radiation pattern. The simple solution of this problem is by increasing the distance of reflector from the radiating antenna up to quarter-wavelength. However, it causes significant increase of antenna thickness. Therefore, the antenna is no longer in low profile, which is unsuitable for some applications with requirement of a compact antenna. To overcome this problem, metasurface structures, e.g., [2], have been widely used as the artificial ground plane. Metasurface structures have been designed to mimic a perfect magnetic conductor at the certain frequency, and consequently, allow a low-profile and unidirectional radiation pattern [3–5]. Accordingly, several scholars have employed metasurfaces to enhance the characteristics of RFID tag antennas. In 2014, a method was

Received 15 April 2019, Accepted 31 May 2019, Scheduled 11 June 2019

* Corresponding author: Son Xuat Ta (xuat.tason@hust.edu.vn).

The authors are with the School of Electronics and Telecommunications, Hanoi University of Science and Technology, Ha Noi, Viet Nam.

introduced to increase reading distances of passive RFID-tag antenna with metasurface [6]. By using the metasurface, the tags can be directly attached onto metal or dielectric materials with high permittivity with almost no degradation in their performances. A dipole was combined with a metasurface to operate at 868 MHz frequency [7]. In [8], a metasurface was applied to design a circularly polarized tag in order to achieve a longer read range for UHF RFID on-body applications. A low-profile RFID tag antenna using compact artificial magnetic conductor (AMC) substrate was presented for metallic objects [9]. The modified rectangular patch type AMC substrate with offset vias was employed to significantly reduce the antenna size. The tag antenna shows relatively tolerant reading distances from 2.4 m to 4.8 m under various platform environments such as a conductive plate or a plastic water container. However, the above mentioned RFID tag antennas using metasurface just yielded a single-band operation. It is well known that different countries have allocated different parts of the radio spectrum for RFID. Accordingly, single-band tag antennas cannot be used in different countries. In [10], a bowtie-dipole tag antenna was incorporated with a recessed cavity with AMC ground plane to provide dual-band operation at European (869.5–869.7 MHz) and Korean (910–914 MHz) passive UHF RFID bands. However, the physics behind the dual-band operation has not been rigorously clarified.

This paper presents a low-profile UHF RFID tag antenna with dual-band unidirectional radiation. The antenna consists of a compact dipole incorporated with a metasurface of 4×4 periodic metallic plates. This incorporation is to not only achieve the low-profile and unidirectional radiation, but also provide dual-band operation. For an easy realization, the printed dipole and metasurface are printed on the top and bottom sides of a thin FR-4 substrate, respectively. In order to accomplish conjugate matching with a UCODE G2XM chip, a modified T-matching network is utilized in feeding structure of the dipole. The antenna features are demonstrated by the commercially available electromagnetic simulation software of ANSYS electronics desktop. For verification, the antenna has been fabricated and tested. Its measured readable range agrees rather closely with the predicted values.

2. ANTENNA DESIGN AND CHARACTERISTICS

2.1. Antenna Geometry

Figure 1 depicts the geometry of the proposed RFID tag antenna, which consists of a printed dipole, a metasurface, and a metallic reflector. The dipole and metasurface are printed on the top and bottom sides of a FR-4 Epoxy substrate with dielectric constant of 4.4, loss tangent of 0.025, and thickness of 0.8 mm. The substrate is suspended above the reflector at a distance of H_a . The metasurface consists of 4×4 periodic metallic plates with periodic of L and gap of g between two adjacent plates. The geometry of the printed dipole is shown in Fig. 2. Each dipole arm consists of a meander-line with enlarged ending for antenna miniaturization [11]. The dipole was fed by a T-matching network [12], which was modified for a conjugate impedance matching with the UCODE G2XM chip [13]. The selected tag-chip has an input impedance of $22 - j195 \Omega$ at 915 MHz. For the complex conjugate matching between the tag chip and the antenna, the input impedance of the proposed antenna must be approximately $22 + j195 \Omega$ at the desired frequency.

The metasurface was designed to act as an AMC surface between the dipole and ground plane, and consequently, achieve a unidirectional radiation and low profile. In order to minimize the unit-cell size, each metallic plate of the metasurface structure contained three slots, as shown in Fig. 2(a). The antenna was characterized via the ANSYS electronics desktop to obtain the conjugate impedance matching with the UCODE G2XM chip at dual frequency bands, a low profile, and a unidirectional radiation. Referring to Fig. 1 and Fig. 2(a), the optimized design parameters of the antenna are as follows: $W_{gnd} = 190$ mm, $L = 34$ mm, $g = 0.89$ mm, $H_a = 15$ mm, $W_a = 9.6$ mm, $L_e = 33$ mm, $W_b = 16$ mm, $L_{bd} = 30$ mm, $W_{bs} = 6$ mm, $L_b = 14$ mm, $L_{sub} = 70$ mm, $W_{sub} = 20$ mm, $W_{b1} = W_{b2} = 3$ mm, $L_{b1} = 5$ mm, $L_{b2} = 13$ mm, $L_{s1} = 13$ mm, $W_{s1} = 0.4$ mm, $g_1 = 1.6$ mm, $g_2 = 0.9$ mm, $W_t = 1.5$ mm, $W_f = 0.5$ mm, $L_f = 14$ mm, $L_t = 5.4$ mm, $W_m = 0.5$ mm, $L_1 = 2$ mm.

2.2. Metasurface Structure

The unit-cell geometry of the metasurface structure is illustrated in Fig. 2(a). The metallic is printed on the bottom side of the FR4 substrate, which is suspended on a perfect electric conductor (PEC) surface

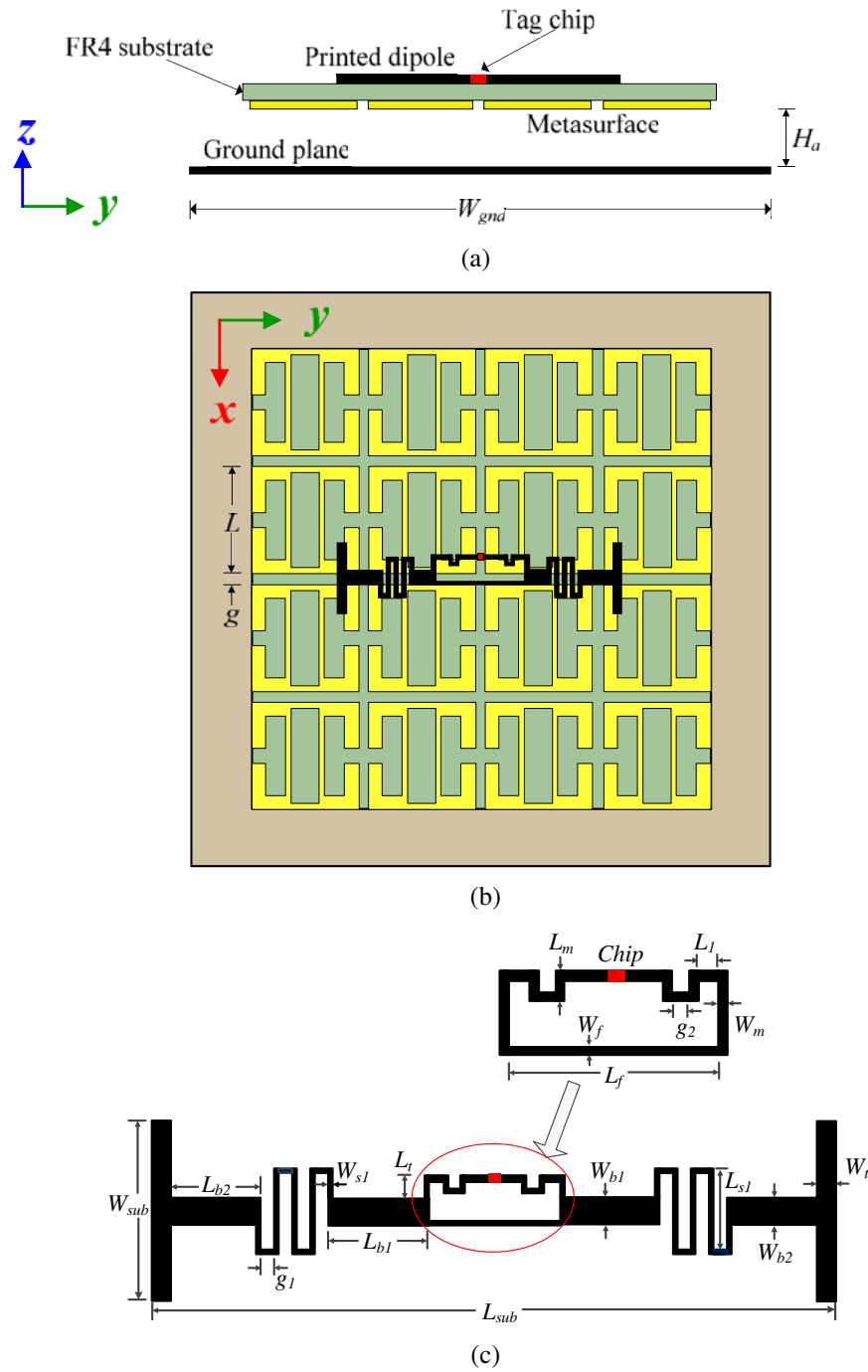


Figure 1. The geometry of proposed tag antenna: (a) side view, (b) top view, and (c) compact printed dipole with modified T-matching network.

via an air gap (H_a). The design evolution of the metallic plate is illustrated in Fig. 2(b); i.e., the initial configuration is a square metallic plate; the second design is a plate with one slot; and the final one is the proposed structure with three slots. All configurations were characterized via the ANSYS Electronics Desktop software with the same conditions of size of unit-cell and FR4 substrate. The reflection phases of three metasurface structures were calculated and given in Fig. 2(c). It is observed that the initial design yielded a resonant frequency of 1039 MHz for the 0° reflection phase. Due to the presence of the slot, the resonant frequency of the metasurface structure shifted toward the low frequency region

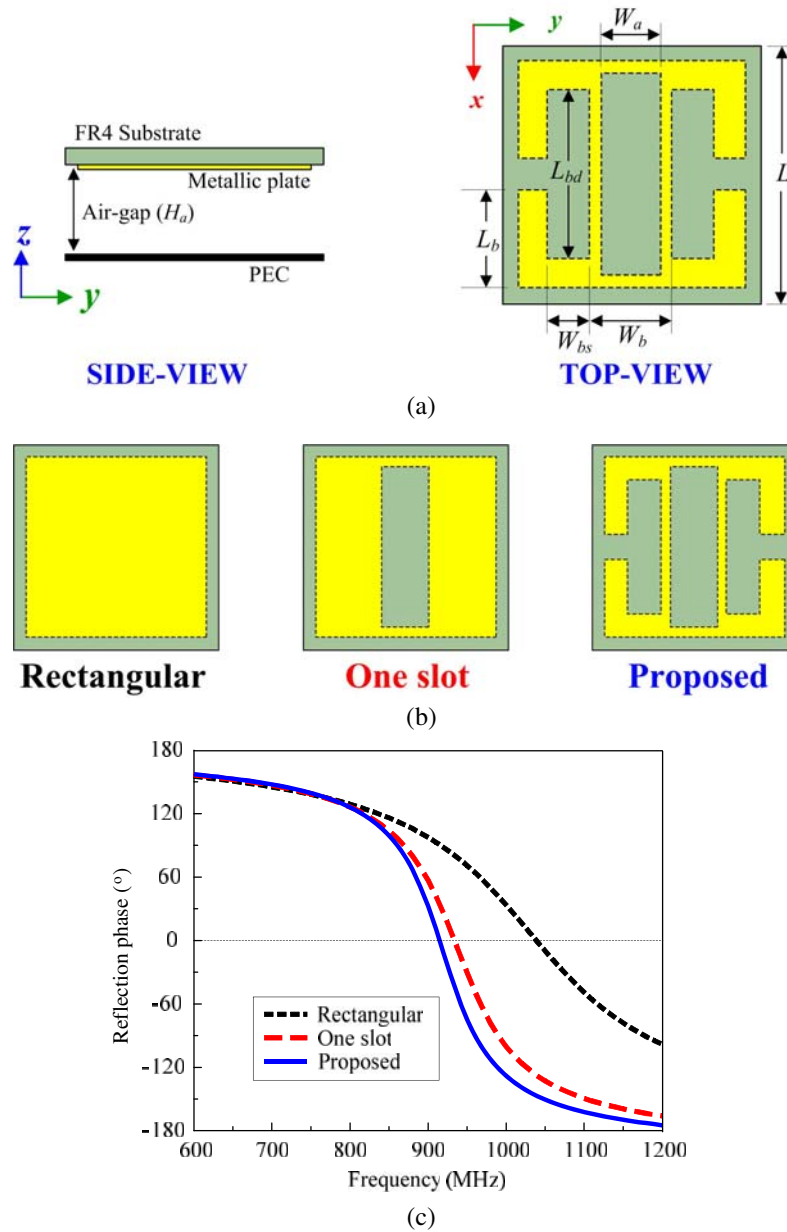


Figure 2. Design of the metasurface structure: (a) geometry of the unit-cell, (b) designing evolution, and (c) reflection phase.

as compared to the initial design. The resonant frequency of the second structure was at 930 MHz. To further reduce the resonant frequency, two T-shaped slots were embedded into the plate of the second design. The proposed structure yielded a resonant frequency of 910 MHz for 0° reflection phase. This indicates that the use of slots on the metasurface structure is one of the miniaturization techniques. From Fig. 2(c), the bandwidth of the proposed metasurface is 850–950 MHz for reflection phase from -90° to $+90^\circ$.

2.3. Dual-Band Operation

For illustrating the advantages, a characteristic comparison between the proposed design and the compact tag dipole antenna in free space was carried out. Both configurations were optimized in

order to obtain a conjugate impedance matching with the UCODE G2XM chip at 925 MHz. The configuration of the printed dipole in free space [Fig. 3] is slightly modified as compared to the proposed design, i.e., it has E-shaped endings and two turns in the T-matching network. Referring to Fig. 3, the optimized design parameters of the dipole in free space are as follows: $L_{sub} = 70$ mm, $W_{sub} = 20$ mm, $L_{t1} = 6$ mm, $R_{t1} = 4$ mm, $L_{b1} = 18$ mm, $L_{b2} = 10$ mm, $W_{b1} = W_{b2} = 3$ mm, $W_{s1} = 0.4$ mm, $g_1 = 1$ mm, $g_2 = 0.09$ mm, $L_{s1} = 10$ mm, $W_t = 1$ mm, $L_t = 2.48$ mm, $L_m = 2.05$ mm, $W_m = 0.54$ mm, $L_f = 15.3$ mm, $W_f = 0.8$ mm, $L_1 = 2$ mm, $W_{ff} = 0.585$ mm. The performance comparison is shown in Figs. 4 and 5.

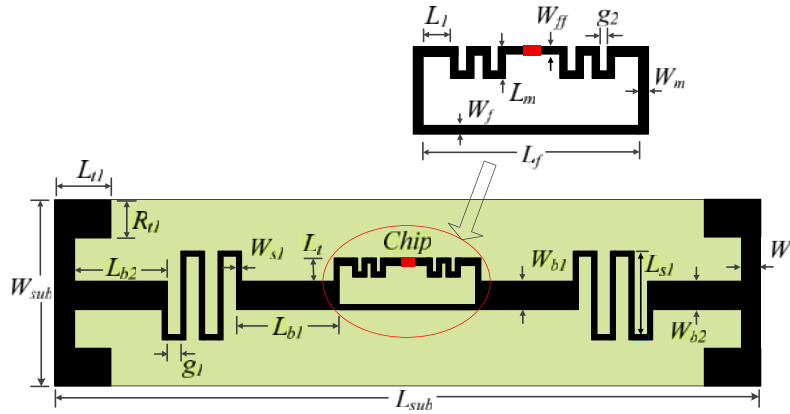


Figure 3. The geometry of the printed dipole antenna in free space.

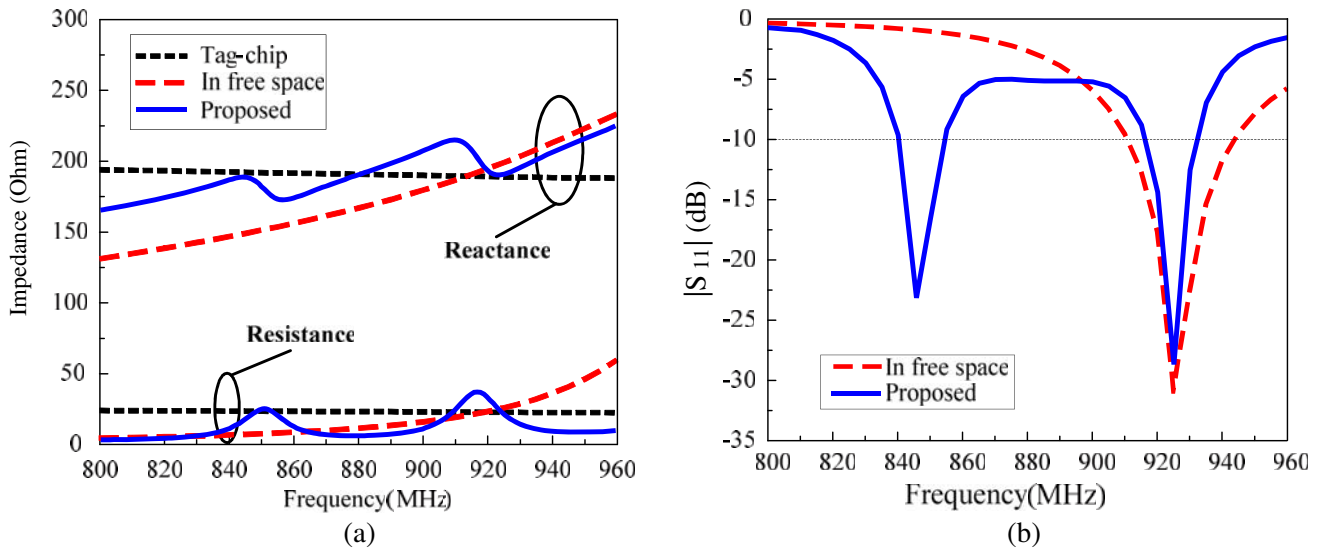


Figure 4. (a) Input impedance and (b) $|S_{11}|$ value of the printed dipoles in free space and with metasurface.

From Fig. 4(a), the input impedance of the dipole in free space yielded one intersection near 925 MHz with the tag chip, whereas the proposed antenna resulted in several corresponding intersections. The dipole in free space yielded $Z_{11} = 22 + j189$ at 925 MHz, while the proposed design yielded $Z_{11} = 19 + j190$ (Ω) at 845 MHz and $Z_{11} = 23 + j192$ (Ω) at 925 MHz. For a better illustration, the reflection coefficient $|S_{11}|$ values of the two configurations were calculated by using the following formula [14].

$$|S_{11}| = -20 \log \left| \frac{Z_a - Z_c^*}{Z_a + Z_c^*} \right| \quad (1)$$

where Z_a and Z_c are the input impedances of the antennas and the tag chip, respectively. The calculated reflection coefficients are given in Fig. 4(b). The dipole in free space exhibited single-band operation with a $|S_{11}| < -10$ dB bandwidth of 34 MHz (910–944 MHz) with one resonance at 925 MHz ($|S_{11}| = -31.0$ dB). The proposed antenna exhibited dual-band operation with a $|S_{11}| < -10$ dB bandwidth of 15 MHz (840–855 MHz) and 18 MHz (916–932 MHz) with two resonances at 845 MHz ($|S_{11}| = -21$ dB) and 925 MHz ($|S_{11}| = -26$ dB). These results demonstrated that the presence of the metasurface produced the dual-band characteristic for the antenna system. Fig. 5 shows the 3-dimension (3D) total-gain radiation of the two antennas. In free space, the printed tag dipole yielded an omnidirectional radiation pattern with a directivity of 2 dB. With the metasurface and ground plane, the antenna achieved a good broadside radiation with high front-to-back ratio and highly symmetric patterns at both resonance frequencies. As shown in Fig. 5(b), the antenna yielded a directivity of 5.8 dB and 7.0 dB for the lower and upper bands, respectively.

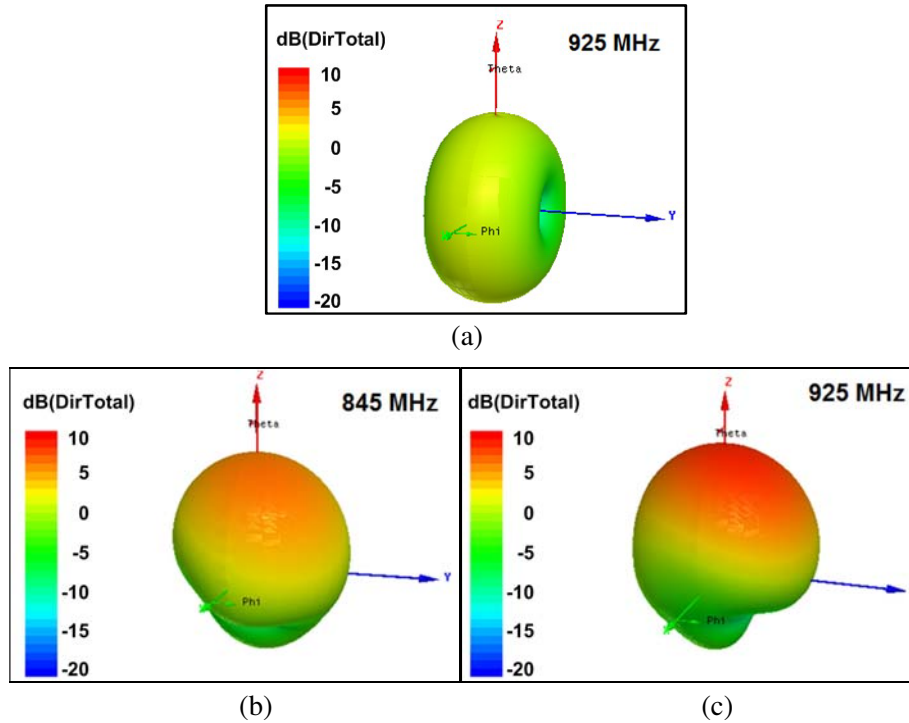


Figure 5. 3D total-gain radiation pattern of the printed dipole at its resonance frequencies: (a) in free space and (b) with metasurface.

In order to clarify the mechanism of the dual-band operation, a parametric study was carried out for different sizes of the metasurface, and the results are given in Fig. 6. It is observed that the metasurface size affected the input impedance of the antenna, as shown in Fig. 6(a). For a better illustration of the effects, the reflection coefficients of the antenna for different numbers of cells were calculated using Equation (1) and shown in Fig. 6(b). As the number of cells increased, the lower resonances changed slightly, whereas the upper resonances significantly shifted toward the lower frequency region. The 2×2 cell configuration resulted in a resonance at 845 MHz ($|S_{11}| = -4.9$ dB), while its upper resonance was out of the examined frequency range. The 4×4 cell configuration (optimized one) resulted in two resonances at 845 MHz ($|S_{11}| = -21$ dB) and 925 MHz ($|S_{11}| = -26$ dB). With 6×6 cells, the antenna resulted in two resonances at 838 MHz ($|S_{11}| = -18$ dB) and 885 MHz ($|S_{11}| = -6$ dB). These results indicated that the resonance caused by the dipole was the lower one, whereas the upper resonance was generated by the metasurface. This phenomenon is due to surface waves propagating on the metasurface, which are excited to generate the extra resonances for the antenna system [15].

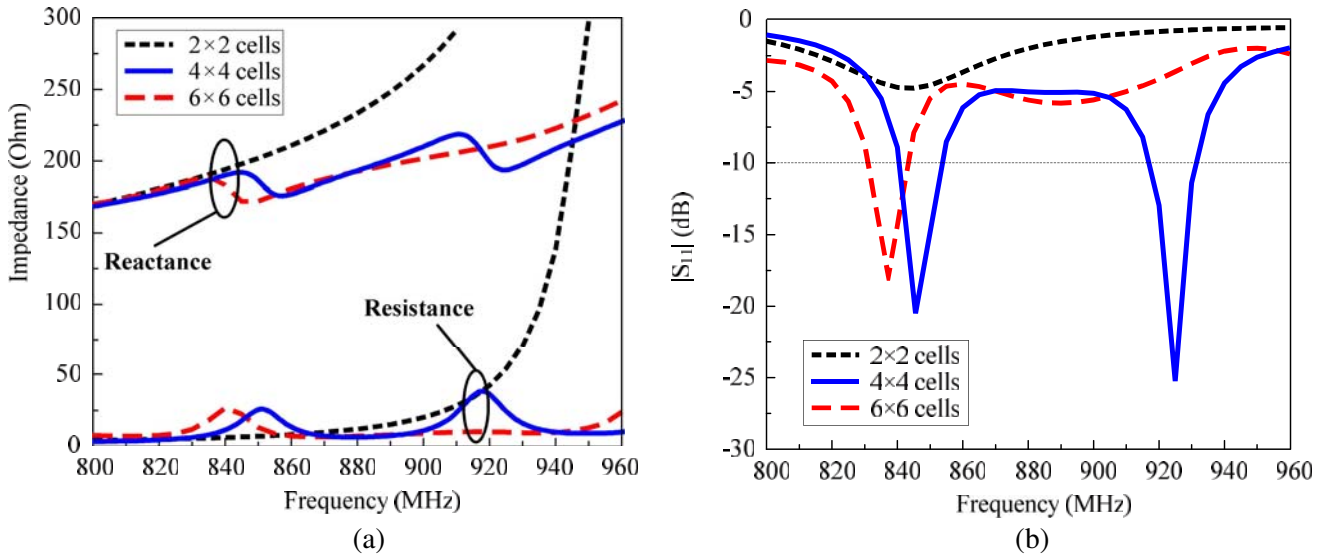


Figure 6. (a) Input impedance and (b) reflection coefficient of the proposed antenna for different sizes of the metasurface.

3. EXPERIMENTAL TEST

The proposed UHF RFID tag antenna using metasurface was fabricated, and its fabricated sample is shown in Fig. 7. The printed dipole and metasurface were realized on an FR4 substrate sheet via the standard printed circuit board technology. Four plastic piles (not included in the simulations) were used to create the air layer between the ground plane and the FR4 substrate.

In order to verify the performances, the measurements for the reading distance of the RFID tag antenna were carried out. Fig. 8 illustrates the measurement setup for the RFID tag antenna. The measurement system includes a computer, a UHF RFID reader module with a reader antenna, and the proposed tag antenna. The reader module is a Thing magic M6e RFID reader module developed by JADAK [16], which was connected to the computer by USB interface. A circular polarization MT-242025/TRH/A/A model [17] was used as the reader antenna, which was connected to the reader module by a 50- Ω coaxial cable. The tag antenna and reader antenna were mounted on two 1.2-m wooden posts and arranged on a line. With the given equipment, based on the Friis transmission equation [18], the maximum readable range of the proposed antenna can be theoretically calculated by using the following formula:

$$R_{\max} = \frac{\lambda_0}{4\pi} \sqrt{\frac{P_t G_t G_{tag} \rho}{P_{tag}}} \quad (2)$$

where R_{\max} is the maximum readable range, P_t the transmitted power of the reader antenna, λ_0 the wavelength in free space, G_t the gain of the reader antenna, G_{tag} the gain of the tag antenna, ρ the loss factor due to the polarization mismatch, and P_{tag} the minimum required power for the tag. The gain of the tag antenna is defined as below:

$$G_{tag} = \eta D_{tag} \quad (3)$$

where η and D_{tag} are the radiation efficiency and directivity of the tag antenna, respectively. Assuming that the loss from the substrate is negligible, the radiation efficiency of the proposed antenna is mainly dependent on the impedance mismatch, and therefore:

$$\eta = 1 - |\Gamma|^2 \quad (4)$$

where Γ is the reflection coefficient of the tag antenna.

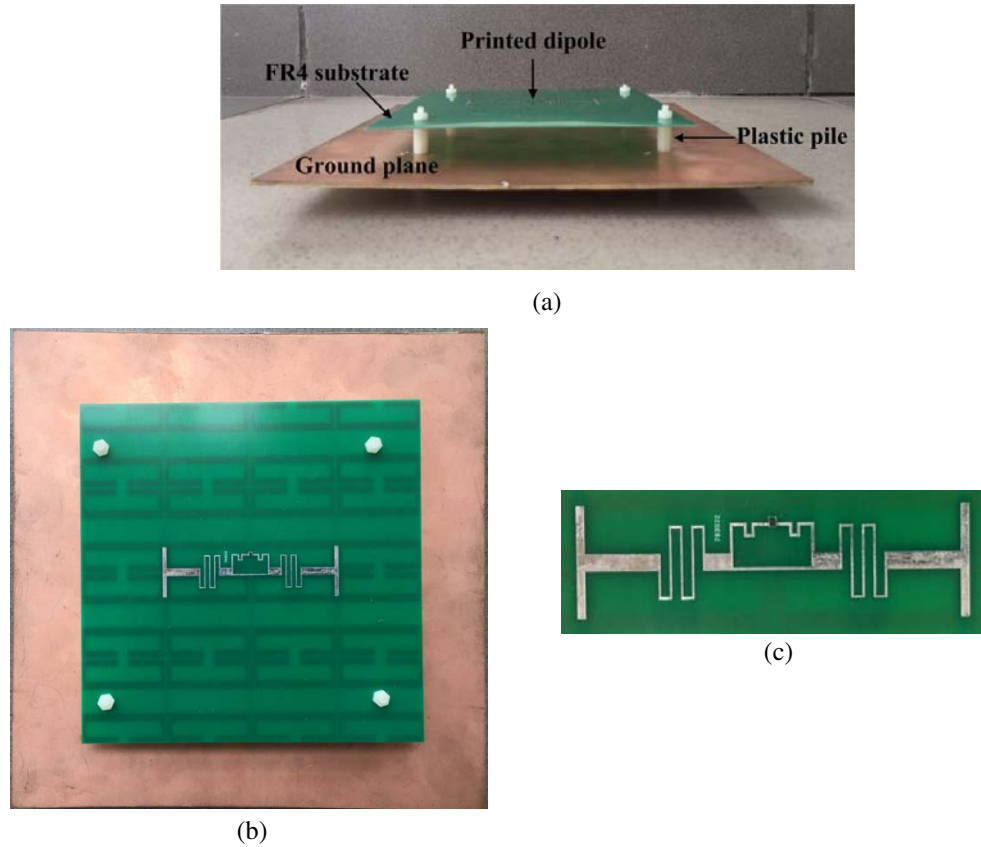


Figure 7. A fabricated sample: (a) perspective view, (b) top view, and (c) printed dipole with tag-chip.

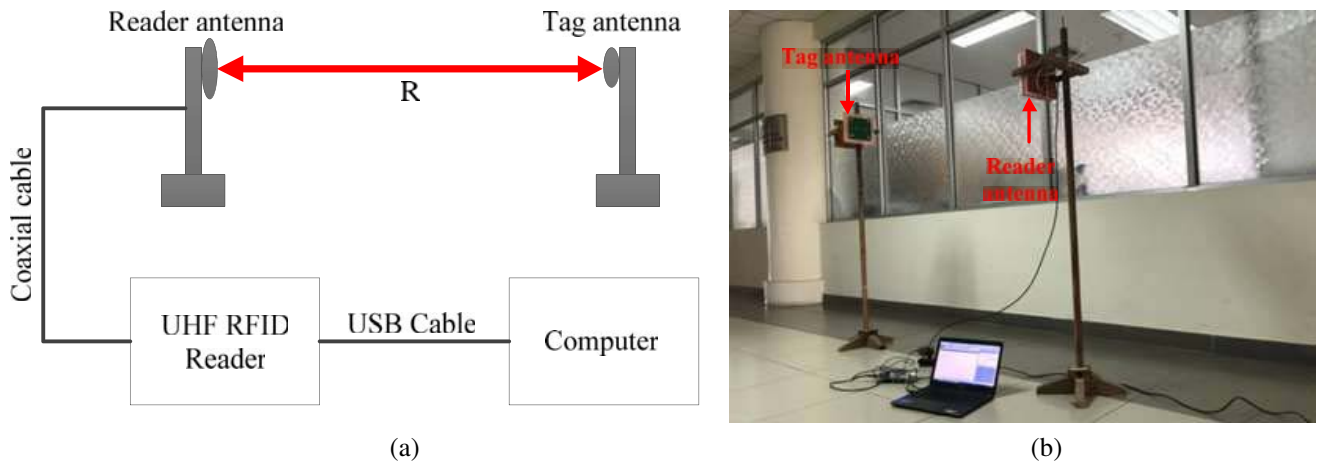


Figure 8. Measurement setup of the RFID tag antenna for readable range: (a) block diagram and (b) photograph.

Insert Eqs. (3) and (4) into Eq. (2), the formula for calculating the maximum readable range is as below:

$$R_{\max} = \frac{\lambda_0}{4\pi} \sqrt{\frac{P_t G_t D_{tag} (1 - |\Gamma^2|) \rho}{P_{tag}}} \quad (5)$$

From the data sheets of the reader module [16], reader antenna [17], and tag chip [13], we have

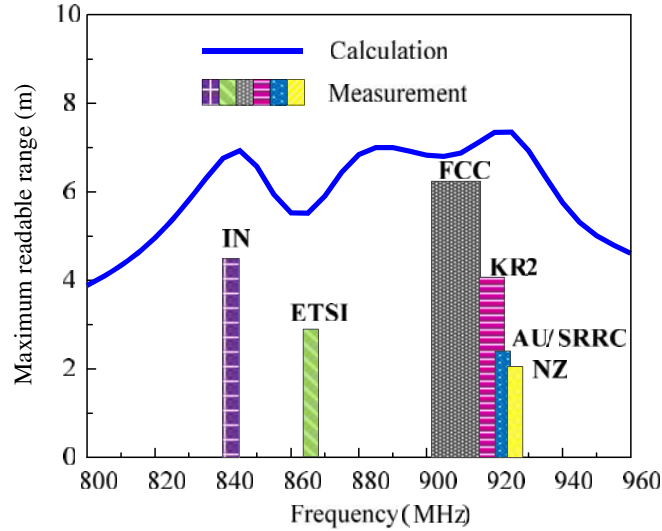


Figure 9. Comparison of the calculated and measured readable ranges.

$P_t = 30$ dBm, $G_t = 7$ dBic, and $P_{tag} = -15$ dBm. Since the reader antenna is circular polarization and tag antenna linear polarization, ρ is assumed to be 0.5. By inserting D_{tag} and Γ exported from the simulations into Equation (5), the maximum readable range was calculated and given in Fig. 9. The calculations resulted in the maximum readable range of 6.9 m and 7.4 m at 845 MHz and 925 MHz, respectively.

The maximum readable range of the fabricated prototype was measured by keeping the tag antenna in motion away from the reader antenna along a straight line up to the point where the received power approximately equals the minimum required power for the tag (P_{tag}). The maximum readable range is measured for the seven standard frequency bands provided by the Thingmagic M6e RFID reader module, including ETSI for European Union (866–869 MHz), FCC for North America (902–928 MHz), SRRC (920–925 MHz) for People’s Republic of China, KR2 (917–923 MHz) for Korea, IN (840–845 MHz) for India, AU (920–925 MHz) for Australia, and NZ (922–927 MHz) for Newzealand. The measured values are shown in Fig. 9, and details are listed in Table 1. Although the measured readable range was not done for the full examined frequency range due to the option limit of the available reader module, the results for different standard frequency bands validate the antenna performances. The fabricated prototype yielded two peak readable ranges at the IN and FCC bands with values of 4.4 m and 6.0 m, respectively. These confirmed the dual-band operation of the proposed antenna. The measurement readable range is lower than the calculation values. This difference could be attributed to some losses from the real FR-4 substrate and the shift (caused by the fabrication tolerance) in the resonant frequencies of the prototype and the predicted values.

Table 1. Measured maximum readable range of the proposed tag antenna at seven standard UHF RFID frequency bands.

Frequency Band	Maximum reading range
IN (840–845 MHz)	4.4 m
ETSI (865–869 MHz)	2.8 m
FCC (902–928 MHz)	6.0 m
KR2 (917–923 MHz)	4.0 m
SRRC (920–925 MHz)	2.2 m
AU (920–925 MHz)	2.3 m
NZ (922–927 MHz)	2. m

4. CONCLUSION

The paper describes a low-profile unidirectional tag antenna with dual-band operation for the UHF RFID applications. It consists of a compact printed dipole, which is incorporated with a metasurface to not only achieve the low-profile and unidirectional radiation, but also provide dual-band operation. Due to using a modified T-matching network, the antenna has a good conjugate impedance matching with the UCODE G2XM chip at the dual frequency. For low cost and easy realization, the dipole and metasurface are built on the top and bottom sides of a thin FR-4 substrate, respectively. The antenna performances have been first optimized by using ANSYS electronics desktop software and confirmed by experiments. The final design with overall size of $190 \text{ mm} \times 190 \text{ mm} \times 15.8 \text{ mm}$ ($0.532\lambda \times 0.532\lambda \times 0.044\lambda$ at 840 MHz) achieved a simulated $|S_{11}| < -10 \text{ dB}$ bandwidth of 15 MHz (840–855 MHz) and 16 MHz (916–932 MHz) and a directivity of 5.8 dB and 7.0 dB at 845 MHz and 925 MHz, respectively. The measurements result in a maximum readable range of 6-m and 4.4-m for FCC (902–928 MHz) and IN (840–845 MHz) standard frequency bands, respectively. With many promising features — including low-profile, simple configuration, dual-band operation, good conjugate matching, unidirectional radiation, low cost, long readable range — the proposed tag antenna could be widely used in the UHF RFID applications.

ACKNOWLEDGMENT

This research is funded by the Vietnam National Foundation for Science and Technology Development (NAFOSTED) under grant number 102.04-2016.02.

REFERENCES

1. Ajami, S. and A. Rajabzadeh, “Radio frequency identification (RFID) technology and patient safety,” *Official Journal of Isfahan University of Medical Sciences*, Vol. 18, 809–813, 2013.
2. Sievenpiper, D. F., L. Zhang, R. F. J. Broas, N. G. Alexopoulos, and E. Yablonovich, “High-impedance electromagnetic surface with a forbidden frequency band,” *IEEE Transactions on Microwave Theory and Techniques*, Vol. 47, No. 11, 2059–2074, 1999.
3. Dewan, R. and M. A. Rahim, “Antenna performance enhancement with artificial magnetic conductor (AMC),” *IEEE Conference on Antenna Measurements & Applications (CAMA)*, Chiang Mai, Thailand, 2015.
4. Abbasi, N. A. and R. J. Langley, “Multiband-integrated antenna/artificial magnetic conductor,” *IET Microwaves, Antennas & Propagation*, Vol. 5, No. 6, 711–717, Apr. 2011.
5. De La Torre, P., J. M. Fernández, and M. Sierra-Castañer, “Characterization of artificial magnetic conductor strips for parallel plate planar antennas,” *Microwave and Optical Technology Letters*, Vol. 50, No. 2, 498–504, Feb. 2008.
6. Kim, D., “Advanced design of RFID tag antennas using artificial magnetic conductors,” *International Symposium on Antennas and Propagation*, Kaohsiung, Taiwan, Dec. 2014.
7. Hadarig, R. C., M. Elena de Cos, and F. Las-Heras, “UHF dipole-AMC combination for RFID applications,” *IEEE Antennas and Wireless Propagation Letters*, Vol. 12, 1041–1044, 2013.
8. Chiu, C. and J. H. Hong, “Circularly polarized tag antenna on an AMC substrate for wearable UHF RFID applications,” *IEEE-APS Topical Conference on Antennas and Propagation in Wireless Communications (APWC)*, 71–74, Verona, Italia, 2017.
9. Kim, D. and J. Yeo, “Low-profile RFID tag antenna using compact AMC substrate for metallic objects,” *IEEE Antennas and Wireless Propagation Letters*, Vol. 7, 718–720, 2008.
10. Kim, D. and J. Yeo, “Dual-band long-range passive RFID tag antenna using an AMC ground plane,” *IEEE Trans. Antennas Propag.*, Vol. 60, No. 6, 2620–2626, Jun. 2012.
11. Ta, S. X., I. Park, and R. W. Ziolkowski, “Crossed dipole antennas: A review,” *IEEE Antennas and Propagation Magazine*, Vol. 57, No. 5, 107–122, Oct. 2015.

12. Tran, H. H., S. X. Ta, and I. Park, "A compact circularly polarized crossed-dipole antenna for an RFID tag," *IEEE Antennas and Wireless Propagation Letters*, Vol. 14, 674–677, 2015.
13. UCODE G2XM Datasheet, NXP Company, May 2019, [Online]. Available: https://www.nxp.com/docs/en/data-sheet/SL3ICS1002_1202.pdf.
14. Nikitin, P. V., K. V. S. Rao, S. F. Lam, V. Pillai, R. Martinez, and H. Heinrich, "Power reflection coefficient analysis for complex impedances in RFID tag design," *IEEE Transactions on Microwave Theory and Techniques*, Vol. 53, No. 9, 2721–2725, Sep. 2005.
15. Costa, F., O. Luukkonen, C. R. Simovski, A. Monorchio, S. A. Tretyakov, and P. M. Maagt, "TE surface wave resonances on high-impedance surface based antennas: Analysis and modeling," *IEEE Trans. Antennas Propag.*, Vol. 59, No. 10, 3588–3596, Oct. 2011.
16. Thing Magic M6e UHF RFID, JADAK A Novanta Company, May 2019, [Online]. Available: <https://www.jadaktech.com/products/rfid/embedded-uhf-rfid-readers/mercury6e-m6e/>.
17. MT-242025/TRH/A/A Reader Antenna, Atlas RFID Store, May 2019, [Online]. Available: https://rfid.atlasrfidstore.com/hubfs/1_Tech_Spec_Sheets/MTI/ATLAS_MTI_MT-242025.pdf.
18. Friis transmission equation, Wikipedia, May 2019, [Online]. Available: https://en.wikipedia.org/wiki/Friis_transmission_equation.